Sleep-Induced Vasomotor Pulsation is a Driver of Cerebrospinal Fluid and Blood-Brain Barrier Dynamics in the Human Brain

Tommi Väyrynen[1,2,3], Johanna Tuunanen[1,2,3], Heta Helakari[1,2,3], Vesa Korhonen[1,2,3], Niko Huotari[1,2,3], Johanna Piispala[2,3,4], Mika Kallio[2,3,4], Vesa Kiviniemi[1,2,3,5]

1. Oulu Functional NeuroImaging (OFNI), Department of Diagnostic Radiology, Oulu University Hospital, Oulu 90029, Finland.

2. Research Unit of Health Sciences and Technology, Faculty of Medicine, University of Oulu, Oulu 90220, Finland.

3. Medical Research Center (MRC), Oulu 90220, Finland.

4. Clinical Neurophysiology, Oulu University Hospital, Oulu 90220, Finland.

5. Biocenter Oulu, Faculty of Biochemistry and Molecular Medicine, University of Oulu, Oulu 90220, Finland

Acknowledgments

This study was funded by Instrumentarium Science Foundation (T.V), Jane & Aatos Erkko Foundation 1,210043 (V.Ki.), Academy of Finland TERVA grants 1-2 314497, 335720 (V.Ki), VTR grants from Oulu University Hospital (V.Ki, V.Ko), The EU Joint Programme – Neurodegenerative Disease Research 2022-120 (V.Ki), Academy of Finland Grant 275342, 338599 (V.Ki), The Finnish Medical Foundation (V.Ki), Finnish Brain Foundation (V.Ki), Uniogs/MRC Oulu DP-grant (H.H), Emil Aaltosen Säätiö (H.H), Pohjois-Suomen Terveydenhuollon tukisäätiö (H.H, V.Ko). We thank CSC – IT Center for Science Ltd., Finland for providing high-performance computational resources used in this study. We further thank Hannu Kinnunen and Oura Health for collaboration. We thank Prof. Paul Cumming of Bern University Hospital for language editing.

Abstract

Sleep is crucial for restoring and maintaining brain tissue homeostasis, primarily through enhanced transport of cerebrospinal fluid (CSF) solutes. Infra-slow (<0.1 Hz) vasomotion, CSF flow, and the electrical potential of blood-brain barrier (BBB) all increase during sleep. While these phenomena have been linked to CSF solute transport, there is little understanding of their interaction as potentials drivers of CSF flow. Therefore, we recorded these three signals in a group of healthy volunteers across sleep-wake states with simultaneous 10 Hz functional magnetic resonance imaging (fMRI) of blood oxygen level dependent (BOLD) contrast, direct current-coupled electroencephalography (DC-EEG), and functional near-infrared spectroscopy (fNIRS). We next investigated the directed coupling patterns between these linked processes according to phase transfer entropy (TE). In the awake state, the electrophysiological BBB potential and water fluctuations predicted vasomotor waves uniformly throughout the brain. In sleep state, results showed a reversal of the direction of this coupling in cerebral cortex, as vasomotor BOLD waves started predicting both CSF and BBB potential shifts. Our findings indicate that vasomotor waves become the primary driver of CSF hydrodynamics and BBB electrical potential in human brain during sleep.

Significance statement

We aimed in this study to identify interactions between vasomotor waves, cerebrospinal fluid (CSF) flow, and electrical potential of the blood brain barrier (BBB) across the sleep-wake cycle. Multimodal imaging of these processes revealed a reversal of the direction of CSF coupling in the transition from wakefulness to sleep. The amplitude of vasomotor waves increased during sleep, which came to predict CSF dynamics and BBB voltage changes, suggesting that vasomotion is the primary driver of CSF flow in human sleep. Given the impairment of CSF transport in various neurological disorders, illuminating the mechanism behind CSF flow could lead to better diagnostic strategies. Our study introduces a novel non-invasive method to investigate the mechanisms of CSF flow in human brain.

Introduction

Sleep induces infra-slow oscillations (<0.1 Hz) in the cerebrospinal fluid (CSF) that help to clear the cerebrocortical parenchyma accumulated solutes and metabolites (Iliff et al., 2012; Xie et al., 2013). These oscillations are believed to arise from the physiological action of noradrenaline (Kjaerby et al., 2022), which induces waves of vasomotor tone in cerebral arteries. This stimulated vasomotor activity could alter the geometry of the perivascular CSF spaces and the density of astrocyte endfeet that plaster the capillaries at the blood-brain barrier (BBB) (Bojarskaite et al., 2023). An abundance of human fMRI studies have consistently shown that the amplitude of vasomotor waves increases as a function of sleep depth, suggesting a direct link between sleep and vasomotor activity (Chang et al., 2016; Fukunaga et al., 2006; Helakari et al., 2022; Horovitz et al., 2008; Liu et al., 2018).

In addition to its effects on vasomotor waves, sleep enhances infra-slow oscillations in direct current-coupled electroencephalogram (EEG) signals (Aladjalova, 1957; Marshall et al., 1996, 1998; Väyrynen et al., 2023). These EEG oscillations reflect the electrical potential between brain tissue and blood, which is influenced by changes in water and electrolyte permeability across the BBB (Hornbein & Sorensen, 1972; Kiviniemi et al., 2017; Nita et al., 2004; Revest et al., 1993; Tschirgi & Taylor, 1958; Voipio et al., 2003). Infra-slow oscillations in the EEG are further coupled to neural brain rhythms, with increasing magnitude of the coupling in the transition to sleep (Monto et al., 2008; Vanhatalo et al., 2004; Väyrynen et al., 2023). Moreover, recent studies have linked slow, synchronized neuronal activity to the enhanced exchange of solutes between interstitial fluid and CSF that occurs during sleep (Chong et al., 2022; Fultz et al., 2019; Vijayakrishnan Nair et al., 2023). Thus, there are at least three types of infra-slow oscillations that increase in amplitude during sleep: vasomotor waves, changes in BBB permeability, and CSF flow. However, the causal associations among these oscillations remain poorly understood.

Previous studies have explored these phenomena mainly with animal experiments using invasive techniques, which can disrupt the pressure-sensitive fluid flow mechanisms that comprise the

glymphatic system (Plog et al., 2019). Moreover, the majority of such studies in animals and humans have investigated the several factors in isolation, thus disregarding their possible interactions. To investigate the physiological driver for sleep-induced increases in brain solute clearance, we have developed a non-invasive, multimodal imaging protocol to observe simultaneously changes in human brain vasomotor waves, BBB dynamics, and CSF flow oscillations. Importantly, we sample the fMRI blood oxygen level dependent (BOLD) signal at 10 Hz, to avoid cardiorespiratory aliasing effects (Huotari et al., 2019). Based on information theory, we undertook predictive driver analytics using phase transfer entropy (TE) (Lobier et al., 2014; Schreiber, 2000) to quantify the directed coupling patterns between the signals in awake and sleep states. Based on previous studies in mice (Bojarskaite et al., 2023) we hypothesized that CSF water signal during sleep are driven by vasomotor waves.

In this study, we used non-invasive multimodal imaging to show that infra-slow BOLD, EEG and water volume changes in NIRS are directionally coupled in human brain. Moreover, we found that resting state BOLD oscillations are the net predictors of EEG and NIRS hydrodynamics in the cerebral cortex during sleep, suggesting that vasomotor waves drive CSF flow and influence the electrophysiological potential across the BBB.

Results

To investigate the interconnected hemodynamic, water, and electrical oscillations in the human brain, we utilized our multimodal neuroimaging setup (Fig. 1a). Our study involved 24 healthy participants, of whom 13 (54%) were females; the male and female groups were both of mean age 25 years (Fig. 1b). Participants underwent two scanning sessions: one during wakefulness and another specifically for sleep evaluation. Sleep classification was performed manually using EEG recordings by experienced neurophysiologists (J.P., M.K.). Extracting continuous sleep state-specific epochs yielded for the entire group a total of 46 minutes of wakefulness, 40 minutes of NREM-1 sleep, and 28 minutes of NREM-2 sleep during active MRI scanning (Fig. 1c).

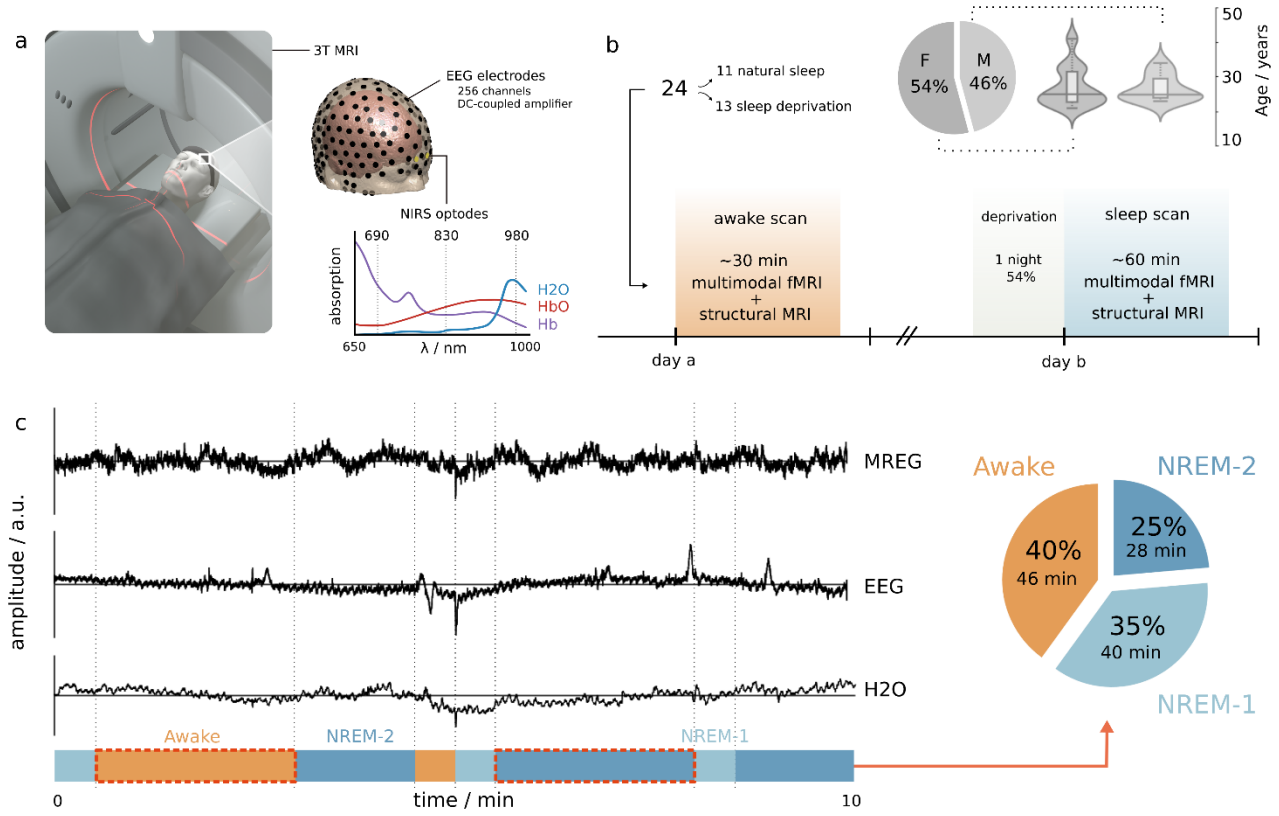

Figure 1. Multimodal imaging protocol for simultaneous measurement of brain water, electrophysiological, and hemodynamic processes. (a) Measurements were conducted in a magnetic resonance imaging (MRI) scanner using a 10 Hz whole-brain magnetic resonance encephalography (MREG) sequence with simultaneous electroencephalography (EEG) and functional near-infrared spectroscopy (NIRS). We applied a water-specific NIRS wavelength (980 nm) to measure brain water concentration changes. (b) Participants underwent two scanning sessions comprising functional MREG and structural scans: one during wakefulness and another during sleep. The pie chart illustrates the gender composition of the (n=24) participants, while the violin plot depicts their age distribution. (c) Representative signals of MREG, EEG, and water NIRS from one participant over a ten-minute period along with corresponding EEG-derived sleep scoring. The pie chart shows the proportions of measurements across three arousal states (awake, NREM-1 and NREM-2) after searching for continuous segments.

Increased infra-slow (<0.1 Hz) hemodynamic and electrical oscillations in sleep.

We first examined the behaviors of the different modalities in the frequency domain, placing a particular focus on the infra-slow range (<0.1 Hz), to test our expectation of increased power across all modalities during sleep. Using two-minute epochs of verified wakefulness and sleep (NREM-1/2), we computed time-frequency estimates (Fig. 2a) within a frequency range of 0.01 to 5 Hz. Visual

examination confirmed a clear differentiation of the three bandwidths: infra-slow, respiratory, and cardiac ranges.

There was a robust power increase in the infra-slow MREG signal in the transition to sleep (Fig. 2b), with a power peak frequency at 0.03 Hz. The group mean infra-slow power was P_A=23.3 (IQR: 23.6) during wakefulness, which increased during sleep to P_{N1}=50.1 (IQR: 36.3) and P_{N2}=52.2 (IQR: 37.8) (A-N1: $Z_{(23,20)}$=-2.59, p_{adj}<0.05*; A-N2: $Z_{(23,14)}$=-3.46, p_{adj}<0.01**). There was a similar trend in EEG signals; the infra-slow power increased from P_A= 1.49 (IQR: 2.34) during wakefulness to P_{N1}=3.73 (IQR: 2.93) and P_{N2}=4.48 (IQR: 3.40) during sleep (A-N1: $Z_{(23,20)}$= -2.42, p_{adj}<0.05*; A-N2: $Z_{(23,14)}$= -2.61, p_{adj}<0.05*). There were no corresponding changes in the NIRS power measurements across arousal states: P_A= 1.15 (IQR: 1.84)*10^{-11}, P_{N1}=1.29 (IQR: 2.38)*10^{-11}, P_{N2}=1.24 (IQR: 4.40)*10^{-11}.

In summary, we detected three distinct oscillation frequency ranges in the 0.01-5 Hz frequency band at baseline, corresponding to infra-slow, respiratory, and cardiac frequency ranges. Consistent with our hypothesis, the power in the infra-slow range increased significantly in MREG and EEG measurements, with greater power as a function of sleep stage. These results indicate parallel increases in vasomotion and voltage potential at the BBB in the transition from awake to sleep states.

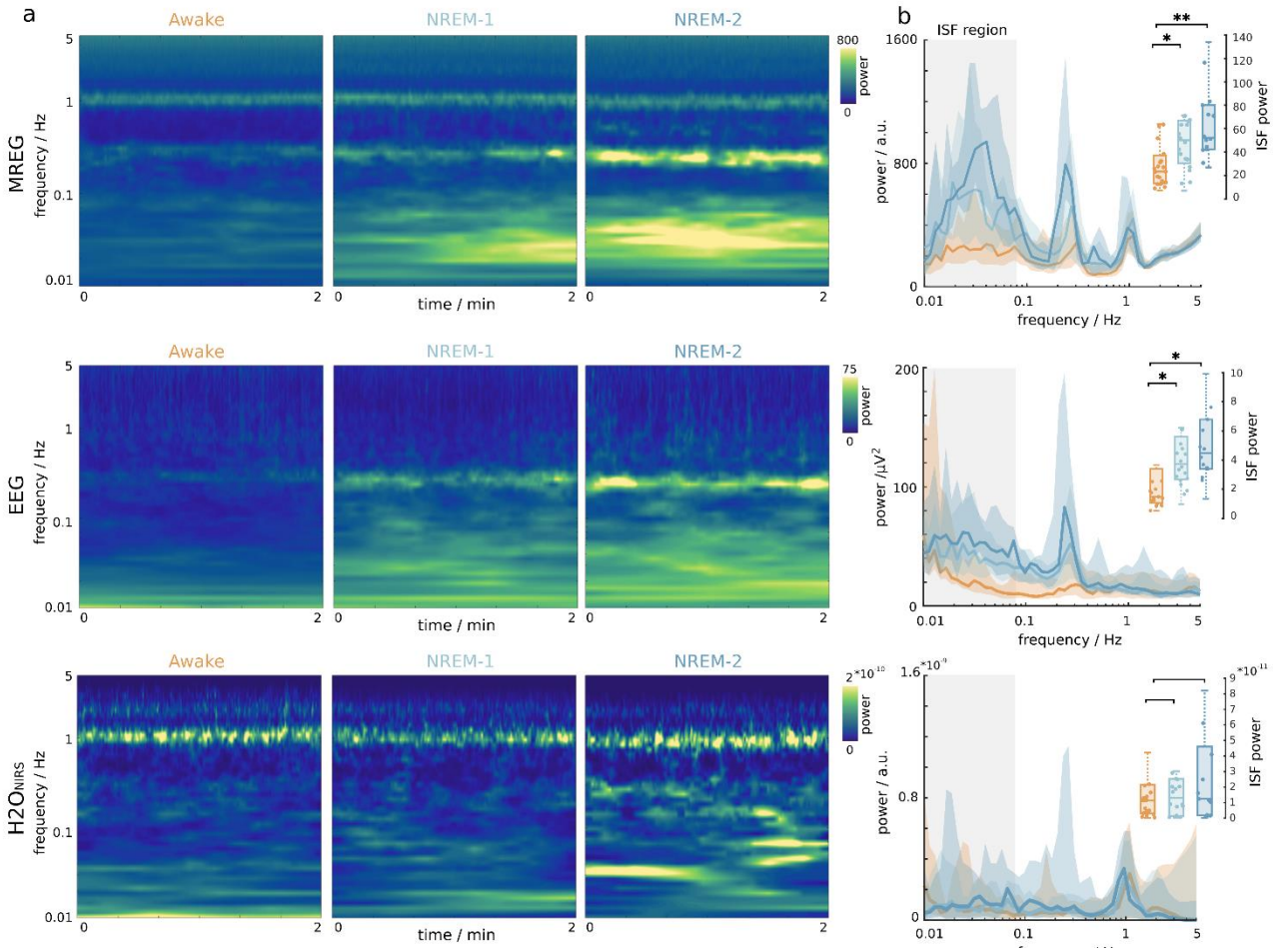

Figure 2. Sleep increases infra-slow power (<0.1 Hz) of magnetic resonance encephalography (MREG) and electroencephalography (EEG). (a) Time-frequency estimates illustrate the average spectral powers for MREG, EEG, and functional near-infrared spectroscopy (NIRS) within sleep state-specific epochs. (b) Time-collapsed power spectra depict frequency as a function of power, where the infra-slow frequency range (0.01-0.08 Hz) serves for statistical comparison. Data points corresponding to wakefulness are denoted by orange, and sleep by light blue (NREM-1) and dark blue (NREM-2). The solid lines represent the median, while the shaded area indicates the middle 50% of data points. Statistical significance is denoted by asterisks (p_{adj}< 0.05*, 0.01**, 0.001***).

Sleep induces local vasomotor drive of brain's infra-slow electrical and water oscillations

We hypothesized that infra-slow vasomotion ($BOLD_{MREG}$) is linked to electrophysiological (BBB_{EEG}) and macroscopic water fluctuations ($H2O_{NIRS}$), with distinct interactions as a function of sleep state. To reveal their coupling patterns, we measured information transfer between the three factors, focusing on phase transitions. We calculated the directed phase-phase coupling according to phase transfer

entropy (TE) in units of bits (Fig. 3a). TE between two variables with no directed relationship is equal to 0 bits.

In awake state, we found that the vasomotor waves of the $BOLD_{MREG}$ signal were predicted by BBB_{EEG} (Fig. 3b) and $H2O_{NIRS}$ (Fig. 3d) phase transitions, as shown by the highly coherent negative net information transfer across the entire brain (indicated by the uniform light blue color in the figure). In both NREM sleep states, there emerged local reversals in the prediction patterns, where $BOLD_{MREG}$ vasomotor waves started predicting the BBB_{EEG} and $H2O_{EEG}$ changes in cortical areas, as indicated by yellow-red colors over the otherwise blue brain. This pattern of positive net information transfer localized over parasagittal areas, encompassing the parietal sensorimotor and temporal regions.

The reversed information transfer of $BOLD_{MREG}$↔BBB_{EEG} coupling during NREM sleep was so widespread that it was also visible in the whole brain averages (Fig. 3c), corresponding to ΔTE_A=-0.11 bit, *IQR*=0.07 bit in wakefulness, which increased to ΔTE_{N1}=1.8*10^{-3} bit, *IQR*=0.09 bit in NREM-1 sleep and to ΔTE_{N2}=-0.01 bit, *IQR*=0.05 bit in NREM-2 sleep. The increased coupling from wakefulness to NREM-1/2 was statistically significant (A-N1: $Z_{23,20}$=-3.4, p_{adj}<0.01**; A-N2: $Z_{23,13}$=-3.7, p_{adj}<0.001***; N1-N2: $Z_{20,13}$=-0.06, p_{adj}=0.96).

Similarly, the $BOLD_{MREG}$↔H_2O_{NIRS} coupling also demonstrated an increasing trend over the whole-brain averages (Fig. 3e). During wakefulness, the median information transfer was ΔTE_A=-0.12 bit, *IQR*=0.20 bit, which increased to ΔTE_{N1}=0.02 bit, *IQR*=0.22 bit during NREM-1 and ΔTE_{N2}=0.27 bit, *IQR*=0.02 bit during NREM-2 sleep. This cortically dominant change was not significant for the whole brain averages: (A-N1: $Z_{22,20}$=-2.4, p_{adj}=0.06; A-N2: $Z_{22,13}$=-1.6, p_{adj}=0.18; N1-N2: $Z_{20,13}$=0.4, p_{adj}=0.87).

The $BOLD_{MREG}$→BBB_{EEG} prediction during transition to sleep showed a wider spatial extent (p_{adj}<0.05) than the smaller but overlapping $BOLD_{MREG}$→$H2O_{NIRS}$ prediction (Fig. 3c,e bottom). Within these reversed prediction areas, 81% of voxels showing a $BOLD_{MREG}$→$H2O_{NIRS}$ prediction increase in NREM-1 also showed a significant increase of $BOLD_{MREG}$→BBB_{EEG}, whereas there was 98% overlap for

NREM-2 sleep. Notably, most subcortical brain regions continued to exhibit negative prediction during sleep, where BBB_{EEG} and $H2O_{NIRS}$ phases still predicted BOLD vasomotion.

We further examined the last candidate of interaction pairs: $BBB_{EEG} \leftrightarrow H2O_{NIRS}$. Here, the topographies demonstrated more stable coupling patterns with respect to arousal state as compared to the other interactions (Fig. 3f). Generally, the central vertex electrodes showed prediction of BBB_{EEG} over $H2O_{NIRS}$, while more peripheral, distal electrodes presented an opposing prediction: $H2O_{NIRS} \rightarrow BBB_{EEG}$. The average ΔTE over all electrodes showed that the prediction $BBB_{EEG} \rightarrow H2O_{NIRS}$ was more dominant, which did not alter with respect to arousal state (Fig. 3e): (A-N1: $Z_{22,20}$=-0.14, p_{adj}=0.9; A-N2: $Z_{22,13}$=-0.29, p_{adj}=0.9; N1-N2: $Z_{20,13}$=0.13, p_{adj}=0.9).

In line with our hypothesis, we found that brain hemodynamics, water, and BBB electrical changes were directionally coupled in all three arousal states studied herein. Wakefulness proved to be the most coherent state, where water dynamics and BBB voltage changes together predicted BOLD vasomotion. Furthermore, BBB potential emerged as a net predictor of water volume changes. In NREM sleep, we found two coexisting mechanisms across brain: the interactions in cortical structures were coordinated by BOLD vasomotion, while deeper brain structures continued to exhibit dynamics similar to the awake state.

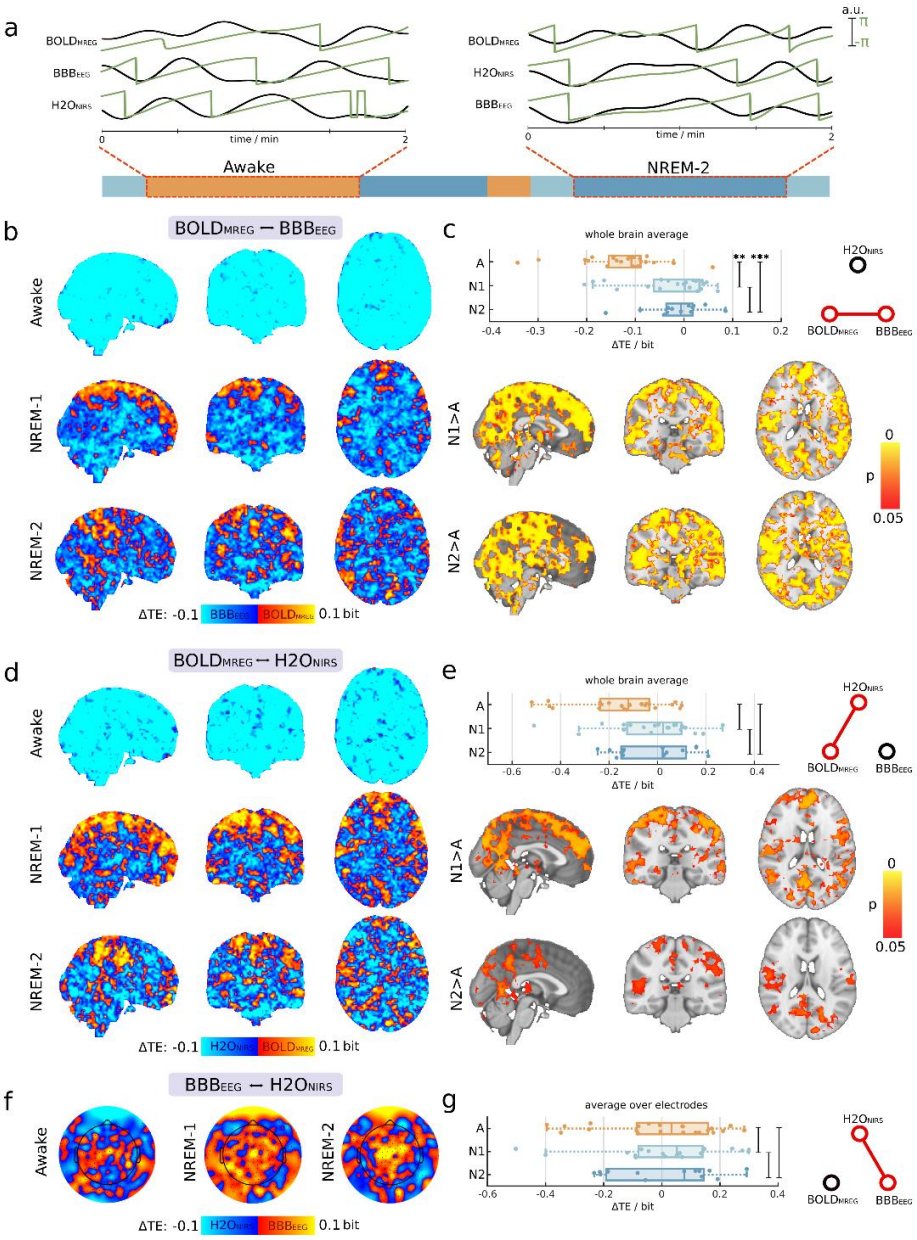

Figure 3. Sleep-induced local cortical reversals in coupling patterns. (a) We utilized the phase time-series (green) of infra-slow signals (black) within sleep state-specific epochs. Transfer entropy in the phase domain (TE) was used to calculate information transfer. The sign of *ΔTE* indicates the net direction of information transfer, as also highlighted in the color bars. (b) Blood oxygen level-dependent ($BOLD_{MREG}$) and electroencephalography (BBB_{EEG}) phases were assessed in wakefulness and NREM-1/2 sleep. Positive values correspond to $BOLD_{MREG}$ prediction, while negative values indicate the net prediction of BBB_{EEG}. (c) We calculated the average TE over the whole-brain volume, where asterisks denote significance of differences (p_{adj}< 0.05*, 0.01**, 0.001***). Below, the spatial distributions of statistically significant areas (p_{adj}<0.05) are shown in comparisons to wakefulness. (d) Similarly, we present TE between $BOLD_{MREG}$ and cortical water dynamics ($H2O_{NIRS}$), where positive values indicate $BOLD_{MREG}$ prediction, and negative values indicate prediction of $H2O_{NIRS}$. (e) Whole-brain averages for

$BOLD_{MREG}$↔$H2O_{NIRS}$ coupling and spatial distribution of significant differences. f) Topographies show coupling patterns between BBB_{EEG} and $H2O_{NIRS}$ and g) average TE taken over electrode space.

Discussion

In this study, we employed a non-invasive multimodal neuroimaging setup to investigate the coupling mechanisms between infra-slow (<0.1 Hz) BOLD vasomotion, electrophysiological and water fluctuations during awake and sleep states. Our findings revealed that these factors exhibit directed coupling dynamics, with differing spatial distributions across arousal state conditions. During wakefulness, infra-slow EEG and water volume changes of fNIRS predicted the BOLD fluctuations across the entire brain. In contrast, during sleep, the coupling dynamics were reversed, with the BOLD signal predicting EEG and water dynamics in dorsal cortical areas. Our findings suggest that vasomotion could be a driving force for increased CSF flow during sleep and influence BBB permeability changes in the cerebral cortex.

Increased Infra-Slow Oscillations in Sleep

Infra-slow oscillations in the BOLD signal are thought to reflect hemodynamic vasomotion (Biswal et al., 1995; Kiviniemi et al., 2000; Rayshubskiy et al., 2014; Silvani et al., 2004; Wang et al., 2008), which has been suggested to drive CSF flow in perivascular spaces, as evidenced by the finding that increased vasomotion amplitude enhances the clearance of β-amyloid in mice (van Veluw et al., 2020). Consistent with previous studies, we found a robust increase in infra-slow BOLD power during sleep, suggesting an increase in vasomotion wave amplitude, which might plausibly indicate enhanced solute clearance (Chang et al., 2016; Fukunaga et al., 2006; Helakari et al., 2022; Horovitz et al., 2008; Liu et al., 2018). The firing rate of cortically projecting locus coeruleus neurons induces infra-slow (0.03 Hz) fluctuations in extracellular norepinephrine levels during NREM sleep, potentially mediating the low frequency vasomotor activity (Kjaerby et al., 2022; Osorio-Forero et al., 2022; van Veluw et al., 2020). Interestingly, the peak spectral power of the BOLD signal also occurred at approximately 0.03 Hz, supporting the idea that the infra-slow BOLD signal reflects these rhythmic oscillations in vascular tone.

Infra-slow range electrical oscillations in DC-EEG signals may arise from a generator in the BBB. Although earlier authors have suggested that neuronal signal sources drive these oscillations, their low amplitude range and the lack of intracortical current loops do not support the neural origin model (Caspers et al., 1987; Nita et al., 2004; Vanhatalo et al., 2003). Changes in cerebral blood flow, pH, and ion trafficking are also associated with infra-slow EEG oscillations (Besson et al., 1970; Caspers et al., 1987; Vanhatalo et al., 2003; Voipio et al., 2003; Woody et al., 1970). Furthermore, the BBB possesses a 5 mV baseline electrical potential (Hornbein & Sorensen, 1972; Revest et al., 1993; Tschirgi & Taylor, 1958) relative to the blood, and changes in permeability of the BBB (which may be voltage-dependent) have been shown to alter infra-slow DC-EEG oscillations (Kiviniemi et al., 2017; Nita et al., 2004; Somjen et al., 1991). Moreover, previous studies have linked sleep state to increased infra-slow oscillations (Marshall et al., 1996, 1998; Väyrynen et al., 2023). In line with those reports, we found increased power of the infra-slow oscillations in NREM-1 and -2 sleep, which could be a marker of increased electrolyte and water trafficking across the BBB.

Recent advancements in fNIRS have enabled the recording of changes in brain CSF water concentration in the subarachnoid space, which is thought to reflect whole brain CSF hydrodynamics (Myllylä et al., 2018). We are not aware of any previous studies of the power changes in CSF dynamics by fNIRS. One important fMRI study reported a pulsatile behavior of CSF flow deep within the 4th ventricle during sleep (Fultz et al., 2019), in support of our hypothesis that cortical CSF hydrodynamic signal measured by fNRIS would behave similarly. Indeed, present results demonstrated infra-slow frequency pulsatile behavior in cortical CSF, which was most pronounced in NREM-2 sleep. The sleep induced power changes in the subarachnoid space and cortex were of lesser magnitude that in the earlier report for the 4th ventricle.

Information Transfer Reveals Novel Interaction Patterns

After having substantiated increased power at infra-slow frequencies in the BOLD and EEG signals during sleep, we aimed to investigate the relationships between infra-slow BOLD and EEG changes, as well as water NIRS. There are various established metrics for studying directed coupling patterns. In this study, we chose transfer entropy, due to its general fitness for analyzing any system without being restricted simply to linear interactions. As a matter of fact, transfer entropy is a nonlinear extension of the well-known Granger causality, and has been shown to outperform other widely used metrics, such as mutual information (Novelli & Lizier, 2021). The key distinction between transfer entropy and the other measures of directed coupling lies in its formulation, which excludes static correlations that can arise from spurious common inputs (Bossomaier et al., 2016).

Previous studies indicated that CSF flow is coupled to the BOLD signal in the 4th ventricle during sleep (Fultz et al., 2019), and during wakefulness (Yang et al., 2022). We now present the first exploration of connections between CSF flow and infra-slow EEG according to arousal state. Our findings confirmed a spatially widespread CSF-BOLD coupling, and furthermore revealed its coordination by the electrical potential across the BBB, as indicated by an information transfer pathway from EEG→H2O→BOLD. During sleep, we detected two coexisting mechanisms, with BOLD vasomotion driving water dynamics in the cerebral cortex, whereas BOLD signals in subcortical structures followed upon DC-EEG and H_2O volume changes. There is a previous report of coupling between CSF inflow and BOLD signal fluctuations decreases as a function of disease severity in patients with Alzheimer-related diseases (Han et al., 2021). Thus, the extent of coupling between CSF flow and BOLD signal fluctuations could also serve as an important predictor for neurodegenerative diseases.

While the coupling of faster neuronal EEG rhythms and BOLD signals is well-established (Logothetis et al., 2001; Pan et al., 2011; Shmuel & Leopold, 2008), few prior studies have focused on the infra-slow domain of DC-EEG. It has been suggested that infra-slow EEG fluctuations coordinate the higher frequency neuronal rhythms (Monto et al., 2008; Vanhatalo et al., 2004; Väyrynen et al., 2023) and

correlate with the resting state BOLD signal (Grooms et al., 2017; Hiltunen et al., 2014; Pan et al., 2013). However, there are no prior studies of the effects of sleep on these dynamics.

It has long been known that changes in cerebral blood flow and BBB permeability are accompanied by infra-slow shifts in DC-EEG. It has been a challenging task to disentangle the source of these oscillations, because any increase in BBB permeability often leads to increased cerebral perfusion, as we have observed during therapeutic intra-arterial mannitol infusions (Kiviniemi et al., 2017). We now show that, the BBB potential drives the resting state BOLD signal in awake human brain. It follows that the regional electrophysiological potential of the BBB likely alters first, presumably leading to changes in hydrodynamics and neurovascular unit activity that drive the regional perfusion changes, rather than the other way around. Herein, we further demonstrated that infra-slow oscillations of DC-EEG do not merely correlate with the BOLD signal in broadly overlapping brain areas, but also exhibit similar dynamics as the BOLD-CSF coupling. Also, the BOLD-EEG coupling showed a reversal in coupling directions upon transition to sleep, suggesting that vasomotion also controls BBB-related potential changes along with hydrodynamics in the cerebral cortex.

We found considerable anatomical overlap between vasomotor drive from the BBB electrical potential and water changes, which could indicate a functional linkage of these couplings to a shared underlying phenomenon. The vasomotor drive of BBB voltage and CSF flow overlaps spatially with slow delta wave increases previously found during light NREM sleep in upper cortical Rolandic regions, which mark a reduction of solute concentration in the cerebral cortex (Helakari et al., 2022). Based on the recent observations of (Bojarskaite et al., 2023), we propose that increased vasomotion may begin to drive the flow of CSF water across the cortical BBB along the perivascular spaces and across astrocytic endfeet gaps via AQP-4 water channels, in association with alterations in the voltage potential over the glia limitans, that is to say between the perivascular space and the brain interstitium.

Future research in the directional couplings reported herein should incorporate more fNIRS channels with deeper subcortical penetration to gain greater information about local water

dynamics. Given the present limitations of direct-current coupled EEG and fNIRS coverage of deeper brain regions, we expect that our present results showed be of greater accuracy in the dorsal brain areas. An intriguing line of future research would be to study these coupling patterns in deep NREM-3 and REM sleep, as might be afforded by prolonged recordings. Additionally, we noted that infra-slow oscillations are transient features, such that probing information transfer over time could provide more insight into the coupling patterns presented herein.

Materials and Methods

Experimental setup

This study was approved by Regional Ethics Committee of the Northern Ostrobothnia Hospital District. We obtained written informed consent from all participants in accordance with the Declaration of Helsinki. The datasets utilized in this study were originally gathered as part of our prior investigation (Helakari et al., 2022, 2023; Väyrynen et al., 2023) involving 24 healthy controls (13 females, 11 males). Participants underwent scanning twice across separate sessions: once during wakefulness and once during sleep. To increase sleep pressure, and thus enable faster onset of the sleep recordings, 13 subjects underwent one night of sleep deprivation, which was monitored with Oura rings (Oura Health Oy). Our study employed a multimodal neuroimaging setup (Korhonen et al., 2014) to capture simultaneous hemodynamic, electrical, and physiological information. We used an MRI scanner to capture functional ultra-fast MREG and structural image series. Spontaneous brain activity was recorded with EEG, which was further used to derive sleep state-specific information. Sleep scoring was performed in 30-second epochs by experienced neurophysiologists according to AASM criteria (J.P., M.K.). Functional NIRS was used to measure changes in macroscopic water concentrations. All modalities were synchronized with the MRI scanner's optical timing pulse. Calculations were performed using MATLAB (v.R2023b, MathWorks).

MRI Acquisition and Preprocessing

Functional and structural images were acquired using a Siemens MAGNETOM Skyra 3T scanner equipped with a 32-channel head coil. For structural 3D MPRAGE scanning (TR=1900 ms, TE= 2.49 ms, TI=900 ms, FA=9°, FOV=240 mm), we used a slice thickness of 0.9 mm. Functional imaging was performed using an ultrafast MREG-sequence (TR=100 ms, TE=36 ms, FA=5°, FOV=192 mm), which employs k-space undersampling to reach a sampling frequency of 10 Hz and voxel size of 3 mm (Assländer et al., 2013). We set a crusher gradient to 0.1, which is optimized for detecting physiological signal sources, while mitigating slow drifts and stimulated echoes.

Reconstruction of MREG images involved the utilization of L2-Tikhonov regularization, wherein a lambda value of 0.1 was determined using the L-curve method (Hugger et al., 2011). Dynamic off-resonance correction in k-space was implemented to reduce B0-field artifacts and mitigate respiratory motion. Image preprocessing followed the standardized FSL (Functional Magnetic Resonance Imaging of the Brain's software library) preprocessing pipeline (Jenkinson et al., 2012). A high-pass filter was used with a cut-off frequency of 0.008 Hz. Subsequently, we performed motion correction followed by brain extraction. To eliminate artifactual spikes, datasets were de-spiked (Cox, 1996). The structural 3D MPRAGE images were used in the registration of functional datasets into the MNI152 standard space. Continuous two-minute segments of wakefulness and NREM-1/2 sleep were identified using sleep scores (Helakari et al., 2023), and filtered to the infra-slow frequency range (0.01-0.08 Hz).

EEG Acquisition and Preprocessing

EEG recordings were acquired using a GES 400 (Magstim EGI) system, which included a direct current-coupled amplifier (Net Amps 400), and a high-density 256-electrode system (HydroCel Geodesic Sensor MR net) with the electrode ‘Cz’ serving as the reference channel. The recordings were conducted at a sampling rate of 1 kHz, except for three sleep and five awake subjects in whom the experimentalists had inadvertently selected 250 Hz. Prior to measurements, we performed a visual inspection of signal quality and electrode impedances.

The initial steps in data processing involved the removal of gradient and ballistocardiographic artifacts through template subtraction ((Allen et al., 1998, 2000), Brain Vision Analyzer v.2.1, Brain Products). Subsequently, bad channels were excluded based on the following criteria: standard deviation exceeding 2000 μV, average correlation with neighboring electrodes falling below 0.1, or electrode impedance surpassing 1 MΩ. Upon identifying bad channels, spherical interpolation was used to replace the removed channels ((Oostenveld et al., 2011) FieldTrip toolbox). EEG signals were decimated to 10 Hz to align with the sampling frequency of other modalities. A zero-phase bandpass filter (0.01-0.08 Hz) was employed using mirrored signals to eliminate filtering edge effects and phase distortions. Finally, measurements were segmented into sleep state-specific epochs.

NIRS Acquisition and Preprocessing

Our functional NIRS device (Myllylä et al., 2018) utilized a frequency-coding technique in which the emitted light was modulated at specific frequencies for each wavelength. High-power LEDs generated monochromatic light at wavelengths of 690, 830, and 980 nm, facilitating measurements of Hb, HbO, and H2O, respectively. Specifically, the 980 nm wavelength was selected for its high absorbance of water, ensuring high sensitivity in water dynamics measurement. At the receiver optode, the light was demodulated again with the corresponding frequencies. To maintain consistent optode positioning, we separated the source and receiver optodes on both sides of the EEG electrode 'Fp1' at a fixed distance of 3 cm, thereby ensuring a constant distance between measurements, while enabling near-infrared light to reach the underlying cerebral cortex (Myllylä et al., 2018).

Initially, NIRS transmittance values were used to compute HbO, HbR, and water concentrations following the modified Beer-Lambert law (Boas et al., 2001; Cope & Delpy, 1988; Myllylä et al., 2018). NIRS concentration signals were decimated to 10 Hz to match the sampling rates of all three modalities. Subsequently, we used a zero-phase recursive bandpass filter (0.01-0.08 Hz) using the mirroring method to isolate the infra-slow frequencies. Finally, we extracted waking and sleep state-specific epochs over the same time points as those for EEG and MREG.

Estimation of spectral properties

We employed complex Morlet wavelets in wavelet convolution to conduct time-frequency spectral analysis (see Fig. 2a,b). These wavelets consist of sine waves at various frequencies tapered by a Gaussian window, thereby providing temporal specificity. Convolving time series with each frequency's wavelet transforms the data into frequency-specific power by computing the squared magnitude of the convolution results. Unlike rectangular windowing, the Gaussian window reduces ripple effects typically associated with sharp edges in the kernel signal. We chose wavelet convolution due to its ability to focus on time-domain changes, its computational efficiency, and its adherence to the assumption of stationarity, contrary to conventional spectral methods (Cohen, 2014). We applied a logarithmic frequency range extending from 0.01 Hz to 5 Hz with 50 steps, having selected the 5 Hz upper limit as it represents the Nyquist frequency of the MREG recordings. To mitigate edge effects that could potentially contaminate the time series, particularly in low-frequency filtering, we implemented the mirroring technique. The number of wavelet cycles (N=8) was held constant, regulating the trade-off between frequency and temporal precision. Given that we had nearly 70,000 spatially-correlating signals in the MREG data, we employed a simple random sampling technique without replacement to reduce computational cost. Here, we used 5% (3,405 voxels) of all voxels, ensuring that each brain voxel had an equal probability of being chosen. Finally, we calculated power in the frequency range of 0.01-0.08 Hz using integral approximation and rectangular windowing.

Inferring directed coupling patterns

Transfer entropy (TE) is a dynamic and directed measure of predictive information (Lobier et al., 2014; Schreiber, 2000). Essentially, TE represents the average information from a source signal that aids in predicting the next value of the target concerning its past. Conditioning in TE can have two opposing effects, either reducing TE by eliminating redundant information between the source and target past, or increasing TE by including synergistic information (Bossomaier et al., 2016; Lizier & Prokopenko, 2010; Wibral et al., 2013). We calculated TE in the phase domain, thereby mitigating effects

of linear mixing and noise (Lobier et al., 2014). To utilize the phase-based TE, we took the infra-slow time series and applied a Hilbert transform to compute the analytical signals $z_{ISF}(n)$. From these analytical signals, we extracted the instantaneous phases as $\theta_{ISF} = arg(z_{ISF}(n))$.

In calculating TE (see Fig. 3), we chose a discrete estimator to represent the state space, being the simplest form of estimators. If the source-target delay is set to maximize information transfer, it aligns with the actual causal delay under simple conditions. However, predictive information can be accurately estimated over a wide range of lags (Lobier et al., 2014). Here, we assumed a constant delay of one cycle, in consideration of the computational cost of identifying the maximal information transfer. We calculated pairwise TE for each MREG voxel, including all EEG electrodes and water concentration signals. To infer the net direction of the information transfer, we took the difference as $\Delta TE(x, y) = TE(x, y) - TE(y, x)$.

Statistical analysis

We had not made a prior statistical power calculation to predetermine the sample size for this study, but used the material at hand. The alpha level was set to 0.05 for all statistical tests. We investigated whether infra-slow power differed between epochs of wakefulness and the combined sleep states (NREM-1/2). A Wilcoxon rank-sum test (two-tailed) was employed with the null hypothesis asserting that awake and sleep epochs had equal infra-slow power (see Fig. 2b). The false discovery rate was controlled using FDR correction (Benjamini & Hochberg, 1995) to account for multiple comparisons. To compare voxelwise group differences in TE, we conducted a randomization test with 5,000 permutations, shuffling the arousal state labels for awake; NREM-1, awake; NREM-2, and NREM-1; NREM-2 (see Fig. 3c, e). Here we used the threshold-free cluster enhancement method to address multiple comparisons. Additionally, to compare whole-brain average TE, we used a Wilcoxon rank-sum test (two-tailed), with the null hypothesis that arousal states had equal median information transfer (see Fig. 3c, e, g). FDR correction was used to control the false discovery rate.

References

Aladjalova, N. A. (1957). Infra-Slow Rhythmic Oscillations of The Steady Potential of the Cerebral Cortex. Nature, 179(4567), 957–959. https://doi.org/10.1038/179957a0

Allen, P. J., Josephs, O., & Turner, R. (2000). A method for removing imaging artifact from continuous EEG recorded during functional MRI. NeuroImage, 12(2), 230–239. https://doi.org/10.1006/nimg.2000.0599 [doi]

Allen, P. J., Polizzi, G., Krakow, K., Fish, D. R., & Lemieux, L. (1998). Identification of EEG events in the MR scanner: the problem of pulse artifact and a method for its subtraction. NeuroImage, 8(3), 229–239. https://doi.org/10.1006/nimg.1998.0361

Assländer, J., Zahneisen, B., Hugger, T., Reisert, M., Lee, H.-L., LeVan, P., & Hennig, J. (2013). Single shot whole brain imaging using spherical stack of spirals trajectories. NeuroImage, 73, 59–70. https://doi.org/10.1016/j.neuroimage.2013.01.065

Benjamini, Y., & Hochberg, Y. (1995). Controlling the False Discovery Rate: A Practical and Powerful Approach to Multiple Testing. Journal of the Royal Statistical Society. Series B (Methodological), 57(1), 289–300. https://doi.org/10.1111/j.2517-6161.1995.tb02031.x

Besson, J. M., Woody, C. D., Aleonard, P., Thompson, H. K., Albe-Fessard, D., & Marshall, W. H. (1970). Correlations of brain d-c shifts with changes in cerebral blood flow. The American Journal of Physiology, 218(1), 284–291. https://doi.org/10.1152/ajplegacy.1970.218.1.284

Biswal, B., Yetkin, F. Z., Haughton, V. M., & Hyde, J. S. (1995). Functional connectivity in the motor cortex of resting human brain using echo-planar MRI. Magnetic Resonance in Medicine, 34(4), 537–541. https://doi.org/10.1002/mrm.1910340409

Boas, D. A., Gaudette, T., Strangman, G., Cheng, X., Marota, J. J. A., & Mandeville, J. B. (2001). The Accuracy of Near Infrared Spectroscopy and Imaging during Focal Changes in Cerebral Hemodynamics. NeuroImage, 13(1), 76–90. https://doi.org/10.1006/nimg.2000.0674

Bojarskaite, L., Vallet, A., Bjørnstad, D. M., Gullestad Binder, K. M., Cunen, C., Heuser, K., Kuchta, M., Mardal, K.-A., & Enger, R. (2023). Sleep cycle-dependent vascular dynamics in male mice and the predicted effects on perivascular cerebrospinal fluid flow and solute transport. Nature Communications, 14(1), 953. https://doi.org/10.1038/s41467-023-36643-5

Bossomaier, T., Barnett, L., Harré, M., & Lizier, J. T. (2016). An Introduction to Transfer Entropy: Information Flow in Complex Systems (1st ed.). Springer International Publishing. https://doi.org/https://doi.org/10.1007/978-3-319-43222-9

Caspers, H., Speckmann, E. J., & Lehmenkühler, A. (1987). DC potentials of the cerebral cortex. Seizure activity and changes in gas pressures. Reviews of Physiology, Biochemistry and Pharmacology, 106, 127–178.

Chang, C., Leopold, D. A., Schölvinck, M. L., Mandelkow, H., Picchioni, D., Liu, X., Ye, F. Q., Turchi, J. N., & Duyn, J. H. (2016). Tracking brain arousal fluctuations with fMRI. Proceedings of the National Academy of Sciences, 113(16), 4518–4523. https://doi.org/10.1073/pnas.1520613113

Chong, P. L. H., Garic, D., Shen, M. D., Lundgaard, I., & Schwichtenberg, A. J. (2022). Sleep, cerebrospinal fluid, and the glymphatic system: A systematic review. Sleep Medicine Reviews, 61, 101572. https://doi.org/10.1016/j.smrv.2021.101572

Cohen, M. X. (2014). Analyzing Neural Time Series Data. The MIT Press. https://doi.org/10.7551/mitpress/9609.001.0001

Cope, M., & Delpy, D. T. (1988). System for long-term measurement of cerebral blood and tissue oxygenation on newborn infants by near infra-red transillumination. Medical & Biological Engineering & Computing, 26(3), 289–294. https://doi.org/10.1007/BF02447083

Cox, R. W. (1996). AFNI: Software for Analysis and Visualization of Functional Magnetic Resonance Neuroimages. Computers and Biomedical Research, 29(3), 162–173. https://doi.org/10.1006/cbmr.1996.0014

Fukunaga, M., Horovitz, S. G., van Gelderen, P., de Zwart, J. A., Jansma, J. M., Ikonomidou, V. N., Chu, R., Deckers, R. H. R., Leopold, D. A., & Duyn, J. H. (2006). Large-amplitude, spatially correlated fluctuations in BOLD fMRI signals during extended rest and early sleep stages. Magnetic Resonance Imaging, 24(8), 979–992. https://doi.org/10.1016/j.mri.2006.04.018

Fultz, N. E., Bonmassar, G., Setsompop, K., Stickgold, R. A., Rosen, B. R., Polimeni, J. R., & Lewis, L. D. (2019). Coupled electrophysiological, hemodynamic, and cerebrospinal fluid oscillations in human sleep. Science, 366(6465), 628–631. https://doi.org/10.1126/science.aax5440

Grooms, J. K., Thompson, G. J., Pan, W.-J., Billings, J., Schumacher, E. H., Epstein, C. M., & Keilholz, S. D. (2017). Infraslow Electroencephalographic and Dynamic Resting State Network Activity. Brain Connectivity, 7(5), 265–280. https://doi.org/10.1089/brain.2017.0492

Han, F., Chen, J., Belkin-Rosen, A., Gu, Y., Luo, L., Buxton, O. M., & Liu, X. (2021). Reduced coupling between cerebrospinal fluid flow and global brain activity is linked to Alzheimer disease–related pathology. PLOS Biology, 19(6), e3001233. https://doi.org/10.1371/journal.pbio.3001233

Helakari, H., Järvelä, M., Väyrynen, T., Tuunanen, J., Piispala, J., Kallio, M., Ebrahimi, S. M., Poltojainen, V., Kananen, J., Elabasy, A., Huotari, N., Raitamaa, L., Tuovinen, T., Korhonen, V., Nedergaard, M., & Kiviniemi, V. (2023). Effect of sleep deprivation and NREM sleep stage on physiological brain pulsations. Frontiers in Neuroscience, 17. https://doi.org/10.3389/fnins.2023.1275184

Helakari, H., Korhonen, V., Holst, S. C., Piispala, J., Kallio, M., Väyrynen, T., Huotari, N., Raitamaa, L., Tuunanen, J., Kananen, J., Järvelä, M., Tuovinen, T., Raatikainen, V., Borchardt, V., Kinnunen, H., Nedergaard, M., & Kiviniemi, V. (2022). Human NREM Sleep Promotes Brain-Wide Vasomotor and Respiratory Pulsations. The Journal of Neuroscience, 42(12), 2503–2515. https://doi.org/10.1523/JNEUROSCI.0934-21.2022

Hiltunen, T., Kantola, J., Abou Elseoud, A., Lepola, P., Suominen, K., Starck, T., Nikkinen, J., Remes, J., Tervonen, O., Palva, S., Kiviniemi, V., & Palva, J. M. (2014). Infra-Slow EEG Fluctuations Are

Correlated with Resting-State Network Dynamics in fMRI. The Journal of Neuroscience, 34(2), 356–362. https://doi.org/10.1523/JNEUROSCI.0276-13.2014

Hornbein, T. F., & Sorensen, S. C. (1972). d-c Potential difference between different cerebrospinal fluid sites and blood in dogs. The American Journal of Physiology, 223(2), 415–418. https://doi.org/10.1152/ajplegacy.1972.223.2.415

Horovitz, S. G., Fukunaga, M., de Zwart, J. A., van Gelderen, P., Fulton, S. C., Balkin, T. J., & Duyn, J. H. (2008). Low frequency BOLD fluctuations during resting wakefulness and light sleep: A simultaneous EEG-fMRI study. Human Brain Mapping, 29(6), 671–682. https://doi.org/10.1002/hbm.20428

Hugger, T., Zahneisen, B., LeVan, P., Lee, K. J., Lee, H.-L., Zaitsev, M., & Hennig, J. (2011). Fast Undersampled Functional Magnetic Resonance Imaging Using Nonlinear Regularized Parallel Image Reconstruction. PLoS ONE, 6(12), e28822. https://doi.org/10.1371/journal.pone.0028822

Huotari, N., Raitamaa, L., Helakari, H., Kananen, J., Raatikainen, V., Rasila, A., Tuovinen, T., Kantola, J., Borchardt, V., Kiviniemi, V. J., & Korhonen, V. O. (2019). Sampling Rate Effects on Resting State fMRI Metrics. Frontiers in Neuroscience, 13. https://doi.org/10.3389/fnins.2019.00279

Iliff, J. J., Wang, M., Liao, Y., Plogg, B. A., Peng, W., Gundersen, G. A., Benveniste, H., Vates, G. E., Deane, R., Goldman, S. A., Nagelhus, E. A., & Nedergaard, M. (2012). A Paravascular Pathway Facilitates CSF Flow Through the Brain Parenchyma and the Clearance of Interstitial Solutes, Including Amyloid β. Science Translational Medicine, 4(147), 147ra111. https://doi.org/10.1126/scitranslmed.3003748

Jenkinson, M., Beckmann, C. F., Behrens, T. E. J., Woolrich, M. W., & Smith, S. M. (2012). FSL. NeuroImage, 62(2), 782–790. https://doi.org/10.1016/j.neuroimage.2011.09.015

Kiviniemi, V., Jauhiainen, J., Tervonen, O., Pääkkö, E., Oikarinen, J., Vainionpää, V., Rantala, H., & Biswal, B. (2000). Slow vasomotor fluctuation in fMRI of anesthetized child brain. Magnetic

Resonance in Medicine, 44(3), 373–378. https://doi.org/10.1002/1522-2594(200009)44:3<373::AID-MRM5>3.0.CO;2-P

Kiviniemi, V., Korhonen, V., Kortelainen, J., Rytky, S., Keinänen, T., Tuovinen, T., Isokangas, M., Sonkajärvi, E., Siniluoto, T., Nikkinen, J., Alahuhta, S., Tervonen, O., Turpeenniemi-Hujanen, T., Myllylä, T., Kuittinen, O., & Voipio, J. (2017). Real-time monitoring of human blood-brain barrier disruption. PloS One, 12(3), e0174072. https://doi.org/10.1371/journal.pone.0174072

Kjaerby, C., Andersen, M., Hauglund, N., Untiet, V., Dall, C., Sigurdsson, B., Ding, F., Feng, J., Li, Y., Weikop, P., Hirase, H., & Nedergaard, M. (2022). Memory-enhancing properties of sleep depend on the oscillatory amplitude of norepinephrine. Nature Neuroscience, 25(8), 1059–1070. https://doi.org/10.1038/s41593-022-01102-9

Korhonen, V., Hiltunen, T., Myllylä, T., Wang, X., Kantola, J., Nikkinen, J., Zang, Y.-F., LeVan, P., & Kiviniemi, V. (2014). Synchronous Multiscale Neuroimaging Environment for Critically Sampled Physiological Analysis of Brain Function: Hepta-Scan Concept. Brain Connectivity, 4(9), 677–689. https://doi.org/10.1089/brain.2014.0258

Liu, X., de Zwart, J. A., Schölvinck, M. L., Chang, C., Ye, F. Q., Leopold, D. A., & Duyn, J. H. (2018). Subcortical evidence for a contribution of arousal to fMRI studies of brain activity. Nature Communications, 9(1), 395. https://doi.org/10.1038/s41467-017-02815-3

Lizier, J. T., & Prokopenko, M. (2010). Differentiating information transfer and causal effect. The European Physical Journal B, 73(4), 605–615. https://doi.org/10.1140/epjb/e2010-00034-5

Lobier, M., Siebenhühner, F., Palva, S., & Palva, J. M. (2014). Phase transfer entropy: A novel phase-based measure for directed connectivity in networks coupled by oscillatory interactions. NeuroImage, 85, 853–872. https://doi.org/10.1016/j.neuroimage.2013.08.056

Logothetis, N. K., Pauls, J., Augath, M., Trinath, T., & Oeltermann, A. (2001). Neurophysiological investigation of the basis of the fMRI signal. Nature, 412(6843), 150–157. https://doi.org/10.1038/35084005

Marshall, L., Mölle, M., Fehm, H. L., & Born, J. (1998). Scalp recorded direct current brain potentials during human sleep. The European Journal of Neuroscience, 10(3), 1167–1178. https://doi.org/10.1046/j.1460-9568.1998.00131.x

Marshall, L., Molle, M., Michaelsen, S., Fehm, H. L., & Born, J. (1996). Slow potential shifts at sleep--wake transitions and shifts between NREM and REM sleep. Sleep, 19(2), 145–151. https://doi.org/10.1093/sleep/19.2.145

Monto, S., Palva, S., Voipio, J., & Palva, J. M. (2008). Very Slow EEG Fluctuations Predict the Dynamics of Stimulus Detection and Oscillation Amplitudes in Humans. The Journal of Neuroscience, 28(33), 8268–8272. https://doi.org/10.1523/JNEUROSCI.1910-08.2008

Myllylä, T., Harju, M., Korhonen, V., Bykov, A., Kiviniemi, V., & Meglinski, I. (2018). Assessment of the dynamics of human glymphatic system by near-infrared spectroscopy. Journal of Biophotonics, 11(8). https://doi.org/10.1002/jbio.201700123

Nita, D. A., Vanhatalo, S., Lafortune, F.-D., Voipio, J., Kaila, K., & Amzica, F. (2004). Nonneuronal origin of CO2-related DC EEG shifts: an in vivo study in the cat. Journal of Neurophysiology, 92(2), 1011–1022. https://doi.org/10.1152/jn.00110.2004

Novelli, L., & Lizier, J. T. (2021). Inferring network properties from time series using transfer entropy and mutual information: Validation of multivariate versus bivariate approaches. Network Neuroscience, 1–32. https://doi.org/10.1162/netn_a_00178

Oostenveld, R., Fries, P., Maris, E., & Schoffelen, J.-M. (2011). FieldTrip: Open Source Software for Advanced Analysis of MEG, EEG, and Invasive Electrophysiological Data. Computational Intelligence and Neuroscience, 2011, 1–9. https://doi.org/10.1155/2011/156869

Osorio-Forero, A., Cherrad, N., Banterle, L., Fernandez, L. M. J., & Lüthi, A. (2022). When the Locus Coeruleus Speaks Up in Sleep: Recent Insights, Emerging Perspectives. International Journal of Molecular Sciences, 23(9), 5028. https://doi.org/10.3390/ijms23095028

Pan, W.-J., Thompson, G. J., Magnuson, M. E., Jaeger, D., & Keilholz, S. (2013). Infraslow LFP correlates to resting-state fMRI BOLD signals. NeuroImage, 74, 288–297. https://doi.org/10.1016/j.neuroimage.2013.02.035

Pan, W.-J., Thompson, G., Magnuson, M., Majeed, W., Jaeger, D., & Keilholz, S. (2011). Broadband Local Field Potentials Correlate with Spontaneous Fluctuations in Functional Magnetic Resonance Imaging Signals in the Rat Somatosensory Cortex Under Isoflurane Anesthesia. Brain Connectivity, 1(2), 119–131. https://doi.org/10.1089/brain.2011.0014

Plog, B. A., Lou, N., Pierre, C. A., Cove, A., Kenney, H. M., Hitomi, E., Kang, H., Iliff, J. J., Zeppenfeld, D. M., Nedergaard, M., & Vates, G. E. (2019). When the air hits your brain: decreased arterial pulsatility after craniectomy leading to impaired glymphatic flow. Journal of Neurosurgery, 1–14. https://doi.org/10.3171/2019.2.JNS182675

Rayshubskiy, A., Wojtasiewicz, T. J., Mikell, C. B., Bouchard, M. B., Timerman, D., Youngerman, B. E., McGovern, R. A., Otten, M. L., Canoll, P., McKhann, G. M., & Hillman, E. M. C. (2014). Direct, intraoperative observation of ~ 0.1 Hz hemodynamic oscillations in awake human cortex: Implications for fMRI. NeuroImage, 87, 323–331. https://doi.org/10.1016/j.neuroimage.2013.10.044

Revest, P. A., Jones, H. C., & Abbott, N. J. (1993). The transendothelial DC potential of rat blood-brain barrier vessels in situ. Advances in Experimental Medicine and Biology, 331, 71–74. https://doi.org/10.1007/978-1-4615-2920-0_12

Schreiber, T. (2000). Measuring Information Transfer. Physical Review Letters, 85(2), 461–464. https://doi.org/10.1103/PhysRevLett.85.461

Shmuel, A., & Leopold, D. A. (2008). Neuronal correlates of spontaneous fluctuations in fMRI signals in monkey visual cortex: Implications for functional connectivity at rest. Human Brain Mapping, 29(7), 751–761. https://doi.org/10.1002/hbm.20580

Silvani, A., Bojic, T., Franzini, C., Lenzi, P., Walker, A. M., Grant, D. A., Wild, J., & Zoccoli, G. (2004). Sleep-Related Changes in the Regulation of Cerebral Blood Flow in Newborn Lambs. Sleep, 27(1), 36–41. https://doi.org/10.1093/sleep/27.1.36

Somjen, G., Segal, M., & Herreras, O. (1991). Osmotic-hypertensive opening of the blood-brain barrier in rats does not necessarily provide access for potassium to cerebral interstitial fluid. Experimental Physiology, 76(4), 507–514. https://doi.org/10.1113/expphysiol.1991.sp003516

Tschirgi, R. D., & Taylor, J. L. (1958). Slowly Changing Bioelectric Potentials Associated With the Blood-Brain Barrier. American Journal of Physiology-Legacy Content, 195(1), 7–22. https://doi.org/10.1152/ajplegacy.1958.195.1.7

van Veluw, S. J., Hou, S. S., Calvo-Rodriguez, M., Arbel-Ornath, M., Snyder, A. C., Frosch, M. P., Greenberg, S. M., & Bacskai, B. J. (2020). Vasomotion as a Driving Force for Paravascular Clearance in the Awake Mouse Brain. Neuron, 105(3), 549-561.e5. https://doi.org/10.1016/j.neuron.2019.10.033

Vanhatalo, S., Palva, J. M., Holmes, M. D., Miller, J. W., Voipio, J., & Kaila, K. (2004). Infraslow oscillations modulate excitability and interictal epileptic activity in the human cortex during sleep. Proceedings of the National Academy of Sciences of the United States of America, 101(14), 5053–5057. https://doi.org/10.1073/pnas.0305375101

Vanhatalo, S., Tallgren, P., Becker, C., Holmes, M. D., Miller, J. W., Kaila, K., & Voipio, J. (2003). Scalp-recorded slow EEG responses generated in response to hemodynamic changes in the human brain. Clinical Neurophysiology, 114(9), 1744–1754. https://doi.org/10.1016/s1388-2457(03)00163-9

Väyrynen, T., Helakari, H., Korhonen, V., Tuunanen, J., Huotari, N., Piispala, J., Kallio, M., Raitamaa, L., Kananen, J., Järvelä, M., Matias Palva, J., & Kiviniemi, V. (2023). Infra-slow fluctuations in cortical potentials and respiration drive fast cortical EEG rhythms in sleeping and waking states. Clinical Neurophysiology, 156, 207–219. https://doi.org/10.1016/j.clinph.2023.10.013

Vijayakrishnan Nair, V., Kish, B. R., Chong, P. L., Yang, H.-C. (Shawn), Wu, Y.-C., Tong, Y., & Schwichtenberg, A. J. (2023). Neurofluid coupling during sleep and wake states. Sleep Medicine, 110, 44–53. https://doi.org/10.1016/j.sleep.2023.07.021

Voipio, J., Tallgren, P., Heinonen, E., Vanhatalo, S., & Kaila, K. (2003). Millivolt-Scale DC Shifts in the Human Scalp EEG: Evidence for a Nonneuronal Generator. Journal of Neurophysiology, 89(4), 2208–2214. https://doi.org/10.1152/jn.00915.2002

Wang, H. H., Menezes, N. M., Zhu, M. W., Ay, H., Koroshetz, W. J., Aronen, H. J., Karonen, J. O., Liu, Y., Nuutinen, J., Wald, L. L., & Sorensen, A. G. (2008). Physiological noise in MR images: An indicator of the tissue response to ischemia? Journal of Magnetic Resonance Imaging, 27(4), 866–871. https://doi.org/10.1002/jmri.21007

Wibral, M., Pampu, N., Priesemann, V., Siebenhühner, F., Seiwert, H., Lindner, M., Lizier, J. T., & Vicente, R. (2013). Measuring Information-Transfer Delays. PLoS ONE, 8(2), e55809. https://doi.org/10.1371/journal.pone.0055809

Woody, C., Marshall, W., Besson, J., Thompson, H., Aleonard, P., & Albe-Fessard, D. (1970). Brain potential shift with respiratory acidosis in the cat and monkey. American Journal of Physiology-Legacy Content, 218(1), 275–283. https://doi.org/10.1152/ajplegacy.1970.218.1.275

Xie, L., Kang, H., Xu, Q., Chen, M. J., Liao, Y., Thiyagarajan, M., O'Donnell, J., Christensen, D. J., Nicholson, C., Iliff, J. J., Takano, T., Deane, R., & Nedergaard, M. (2013). Sleep drives metabolite clearance from the adult brain. Science (New York, N.Y.), 342(6156), 373–377. https://doi.org/10.1126/science.1241224

Yang, H.-C. (Shawn), Inglis, B., Talavage, T. M., Nair, V. V., Yao, J. (Fiona), Fitzgerald, B., Schwichtenberg, A. J., & Tong, Y. (2022). Coupling between cerebrovascular oscillations and CSF flow fluctuations during wakefulness: An fMRI study. Journal of Cerebral Blood Flow & Metabolism, 42(6), 1091–1103. https://doi.org/10.1177/0271678X221074639